Spatial Resolution Enhancement of Hyperspectral Images from Miniaturized Sensors

Sivert Bakken[a,c], Dennis D. Langer[b], Joseph L. Garrett[c], Steven Yves Le Moan[d], and Tor Arne Johansen[c]

[a]SINTEF OCEAN AS, Trondheim, Norway
[b]NTNU, Department of Marine Technology, Trondheim, Norway
[c]NTNU, Department of Engineering Cybernetics, Trondheim, Norway
[d]NTNU, Department of Computer Science, Gjøvik, Norway

ABSTRACT

Here we describe and mitigate issues of optical aberrations related to wavelength-dependent blur caused by miniaturization in hyperspectral pushbroom image sensors, which degrade spatial resolution and limit their usefulness. Panchromatic sharpening algorithms are modified to enhance the spatial resolution of acquired hyperspectral image cubes, explicitly focusing on optical aberrations associated with pushbroom scanners. The study explores algorithms for component substitution and multi-resolution analysis, such as modulation and Laplacian pyramids, adapting them for single image cubes while considering the characteristics of miniaturized hyperspectral imagers. Simulations demonstrate the method's effectiveness in improving the spatial quality of images obtained from miniaturized hyperspectral imagers, expanding their potential applicability. The study evaluates the method using metrics like the BRISQUE score and utilizes data from the HYPSO-1 CubeSat platform.

Keywords: Sharpening, Hyperspectral, Miniaturization, CubeSat

1. INTRODUCTION

Hyperspectral images contain information about the spectral characteristics of the objects in a scene, as revealed by the wavelengths of light they reflect or emit.[1] This information can be used to identify and classify objects in the scene. However, the spatial resolution of a hyperspectral image is often less fine than that of an RGB optical imaging system of similar size. This coarser spatial resolution is making it challenging to see finer details in a remotely sensed scene.[2,3]

This work defines a miniaturized optical imager as a small, compact imaging device. The correlation between size and imaging artifacts is not immediately apparent. While a more miniature imager may not have artifacts, it may require costly components. This work focuses on imaging systems that have prioritized other objectives in the optomechanical design higher than removing optical aberrations, such as spatio-spectral resolution and range. Miniaturized optical imagers are generally smaller than traditional optical imaging systems and can be easily integrated into many devices and systems.[4] These images are ideal for applications where size and weight are important factors, such as Earth Observation from small satellite systems or drone flights.[4,5,6] However, using a miniaturized optical imager has a few potential drawbacks. The smaller size of the imaging components can result in reduced light-gathering ability and fewer degrees of freedom to alleviate optical aberrations.[1] Miniaturized optical imagers may be more sensitive to motion and vibration, which can cause image blur and degradation.[2,4] Further challenges arise when it comes to balancing between spatial, spectral and temporal resolution, especially in the case of the often-used push-broom design.[1,2,4,7,8] The optical aberrations of a push-broom design have been extensively studied and are understood to some extent.[4,8]

Further author information: (Send correspondence to S.B)
S.B: E-mail: sivert.bakken@ntnu.no

Image sharpening is a set of techniques to enhance spatial resolution in remote sensing.[3,9,10,11,12,13] Hyperspectral image sharpening consists of improving, post-acquisition, the spatial resolution of every recorded wavelength. These techniques include spatial filtering, interpolation, and image registration. These techniques can help to sharpen the image and make it easier to see finer spatio-spectral details, such as the edges of objects or other small features in a given scene. Sharpening the images can be helpful for applications where high spatial resolution is beneficial, such as surveillance, environmental monitoring, and geological mapping.

Unlike a hyperspectral image, a panchromatic image is a single-band image that blends light across a wide range of wavelengths.[3,11,13] Panchromatic imaging systems can provide more detailed spatial features compared to a similarly sized hyperspectral imaging system. Panchromatic sharpening is a set of techniques to enhance the spatial resolution of multi- or hyperspectral images using a panchromatic image of the same scene as a reference. This set of techniques combines information from multiple satellite images to produce a single image with high spectral and spatial resolution. This combination can be done using images from different sensors or captured at different times or angles.[3] However, the closer the imaging conditions compare the better the methods is expected to perform. The resulting image can have higher spatial resolution and more detailed information about the various spatial features. These methods require multiple cameras and camera designs that resolve most optical aberrations optomechanically.

The performance of classical panchromatic sharpening algorithms under ideal conditions reliably provide good results.[3,11,13] These algorithms aim to reconstruct high resolution hyperspectral images by combining low spatial resolution hyperspectral images with panchromatic images. In recent years, machine learning and variational optimization-based methods have been proposed as innovative solutions to the panchromatic sharpening problem.[13] Despite utilizing state-of-the-art approaches, these solutions have yet to achieve outstanding results compared to some baseline methods proposed decades ago in the classical panchromatic sharpening literature.

These algorithms typically assume that images have consistent spatial and spectral resolutions across all wavelengths. However, this is only sometimes the case for miniaturized hyperspectral imagers, as they may suffer from various optical aberrations. This study aims to investigate whether the intrinsic values of hyperspectral image cubes can enhance their quality and usability by adapting classical panchromatic sharpening algorithms.

The research presented here offers a preliminary examination of how classical algorithms for panchromatic sharpening and related methods can be applied to enhance images captured by miniaturized hyperspectral imagers that encounter wavelength-dependent spatial blur. The underlying assumption is that some optical aberrations can be compensated using the intrinsic values in the acquired image cube. These findings could enhance the effectiveness of miniaturized sensors in diverse environments and platforms by mitigating some of the common adverse effects of wavelength-dependent blur through post-acquisition processing.

In section 2, a discussion on the expected optical aberrations of miniaturized hyperspectral image sensors describes the simulated hyperspectral scenes and reviews the explored panchromatic sharpening algorithms and the spatial quality assessment metrics. section 3 describes how the aforementioned algorithms are adapted and the underlying assumptions that justify the adaption.

2. BACKGROUND AND REVIEW

This section will cover the background theory of the methods. section 2.1 details the optical aberrations that may occur in a push-broom imaging design. sections 2.3 to 2.5 give a brief overview of the different sharpening algorithms that were deemed potentially useful for the specific system and how they were adapted for testing.

2.1 Pushbroom Imaging and Known Optical Aberrations

A popular design for hyperspectral imaging systems for remote sensing operated by satellites and aerial vehicles is the push-broom design.[4,8] This hyperspectral imager design will be the focus of this paper. The pushbroom design provides certain advantages for mobile imaging platforms. This design also produces some known optical aberrations. These aberrations include such effects as smile and keystone, where pixel misregistration can occur in both spatial and spectral domains. Another common optical aberration in miniaturized hyperspectral

sensors is the non-homogeneous intensity distribution, which often displays a reduction of light intensity on the edges. However, these are often compensated for by applying calibration coefficients.

In a pushbroom imaging system, optical aberrations can also cause the spatial resolution to vary depending on the wavelength of light. These aberrations can arise from lens design, manufacturing imperfections, or environmental conditions. Chromatic aberration causes color fringing or blurring at the image plane due to different wavelengths of light having slightly different refractive indices when passing through a lens. In a pushbroom imaging system, the image is formed by scanning a scene with a linear array of detectors while the system moves along a path. Each pixel in the focal plane array corresponds to a specific wavelength or spectral band; thus, different wavelengths will experience different degrees of blurring or focus at the detector plane. This work adapts various methods used in panchromatic sharpening to improve the quality of the entire hyperspectral image cube by utilizing the sharper wavelengths of the cube as a proxy for the panchromatic image.

2.2 HYPSO-1 Data

The motivation of this study is to enhance data from miniaturized sensors. As a case study, we focus on the hyperspectral imager onboard the HYPSO-1 6U cubesat.[5] We used 20 images of various scenes captured with this platform, a selected subset of which is given in fig. 1. These have also been used to explore the effects of various camera parameters, e.g., exposure time, frame rate, and viewing angle, on the estimated spatial resolution of a scene.[2] In previous work aimed at characterizing the spatial resolution of HYPSO-1 images, the Full-Width at Half-Maximum (FWHM) was found to be in the range of 2.2 pixels.[2,14] Some of the analysis to derive that estimate is given here as the baseline measurement in the results. It has been previously demonstrated that the highest spatial resolution of the HYPSO-1 imager is achieved in the middle of its spectral range, at about 550 nm.

2.3 Component Substitution by Principal Component Analysis

Component substitution is a widely used method for panchromatic sharpening.[3,9] In this method, the spatial component of the hyperspectral image is replaced with the panchromatic image. Histogram matching is a technique that makes the difference between the high-resolution panchromatic and the most significant component of the original image cube as small as possible.

The image cube is first decomposed into components (linear combinations of bands) to perform component substitution with histogram matching. This paper uses Principal Component Analysis (PCA) to perform the transformation. The first component contains the most information and will be substituted by the sharpest band to achieve a sharpening of the entire image cube. The panchromatic image is then usually resampled to a similar resolution as the image cube. With a miniaturized sensor and the poorer spatial resolution resulting solely from optical aberration, we do not need to perform the resampling as the image cube already has the exact image resolution, irrespective of the spectral band. Histogram matching is applied to the original image of the sharpest band, the substitute panchromatic image, to make its histogram similar to that of the first and most significant component of the image cube that PCA transforms. The first component of the image cube is then replaced with the histogram-matched[15] sharpest band and inversely transformed by PCA to create a high-resolution hyperspectral image cube.

In mathematical terms, this can be expressed as follows:

Firstly the hyperspectral image cube I_{cube} of $M \times N$ spatial pixels and p wavelengths is reshaped into a two-dimensional matrix with the spatial elements as rows and the wavelengths as columns, that is,

$$I_{cube} = \begin{bmatrix} \tilde{\mathbf{v}}_{1,1} & \tilde{\mathbf{v}}_{1,2} & \cdots & \tilde{\mathbf{v}}_{1,N} \\ \tilde{\mathbf{v}}_{2,1} & \ddots & \ddots & \vdots \\ \vdots & \ddots & \ddots & \vdots \\ \tilde{\mathbf{v}}_{M,1} & \cdots & \cdots & \tilde{\mathbf{v}}_{M,N} \end{bmatrix}, \qquad \text{reshape}(I_{cube}) = \mathbf{X}_{cube} = \begin{bmatrix} \tilde{\mathbf{v}}_{1,1} \\ \tilde{\mathbf{v}}_{2,1} \\ \vdots \\ \tilde{\mathbf{v}}_{1,2} \\ \vdots \\ \tilde{\mathbf{v}}_{M,N} \end{bmatrix}.$$

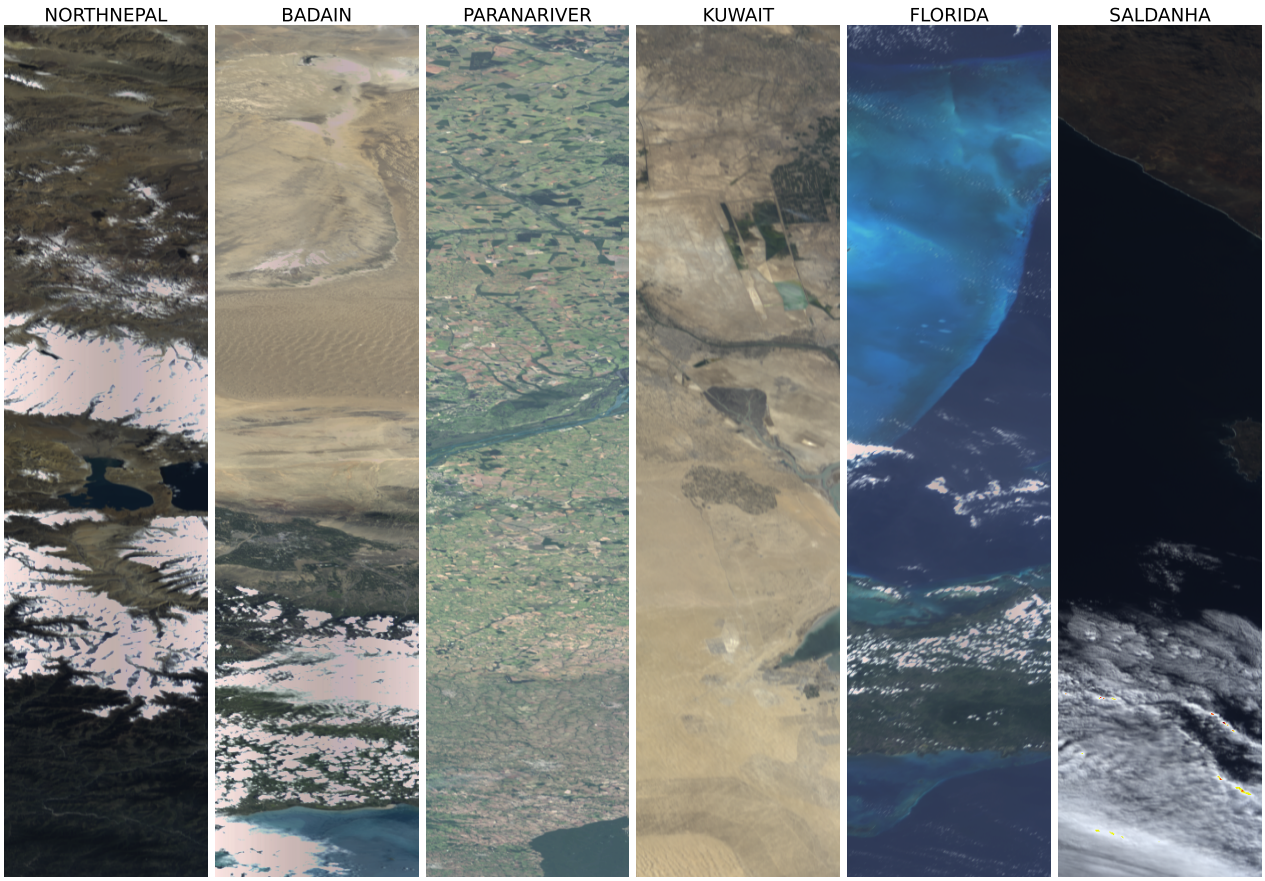

Figure 1: Selected scenes from the HYPSO-1 CubeSat used in this study. The images show various remotely sensed scenes that have distinguishable spatial features. They are rendered as RGBs using the wavelengths 603 nm, 564 nm, and 498 nm, respectively.

Furthermore, the singular value decomposition (SVD) provides the ordered principal components. The first principal component is then replaced with a histogram-matched sharpest band and reconstructed.

An illustration of how the various principal components look is shown in fig. 2. Furthermore, the difference between the first principal component and the histogram-matched center band can be seen in fig. 3.

2.4 Multi-resolution Analysis by Laplacian Pyramid

By multi-resolution analysis, we refer to a method known as the Laplacian pyramid. The generalized Laplacian pyramid is a linear, invertible image representation consisting of band-pass and low-frequency Images. It is used in image sharpening to obtain a fused product with high spatial resolution.

The Laplacian pyramid can be used to improve the sharpness of an image when a reference image is available, e.g., a panchromatic image or a hyperspectral image cube where one of the bands is sharper than the others. This method resembles the Gaussian pyramid, representing the same image at multiple scales. These representations are often produced by using simple low-pass filtering and decimation techniques. The Laplacian pyramid differs by saving the different images of the blurred versions between each level. Only the lowest level, i.e., the sharpest image, is not a different image. This approach enables the algorithm to reconstruct the higher resolution features found in the sharpest image to the other images in the cube via the different images.

The sharpening is done by first constructing the Laplacian pyramid of the original image and the reference image. Then, the Laplacian pyramid of the original image is modified by adding the difference between the

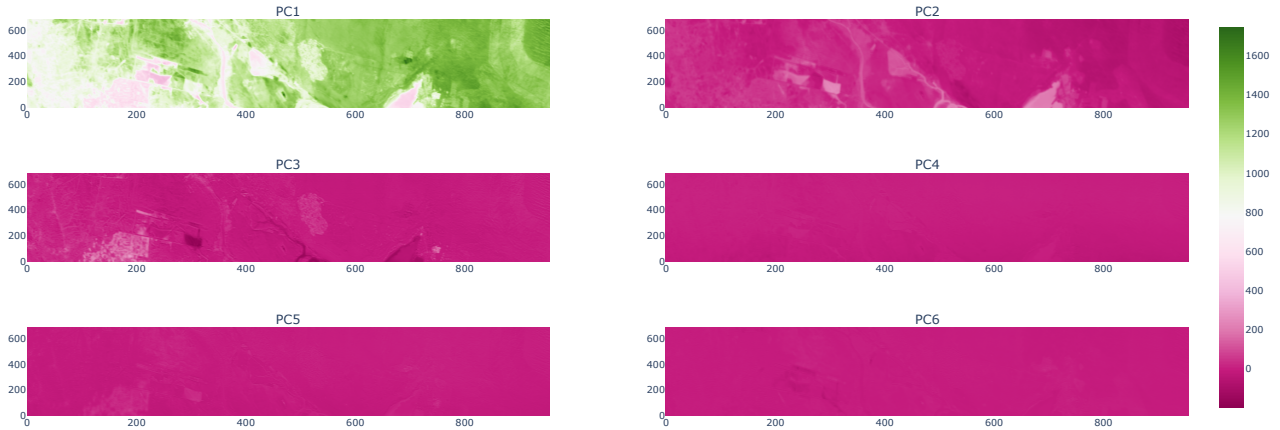

Figure 2: The first six principal components found in the re-projected subspace of the hyperspectral Parana River image cube. Note that most of the *energy* in the components is located in the initial principal component.

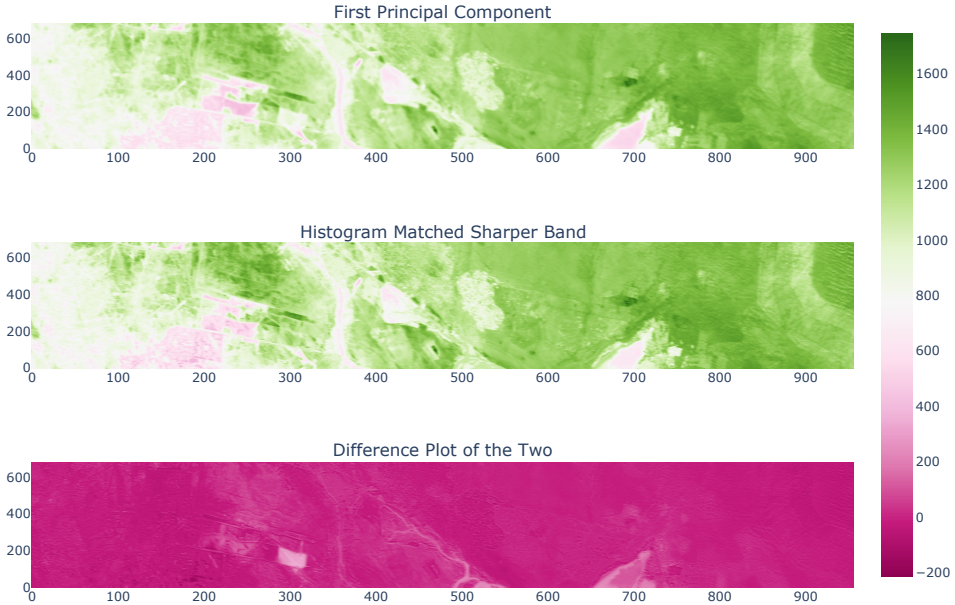

Figure 3: Comparison of the first principal component and the histogram matched center band.

corresponding levels of the Laplacian pyramids of the original and reference images. An illustration of how the different steps affect a given 2D image is given in fig. 4, where the baseband refers to the spectral wavelength that is to be sharpened and the reference band is, in this case, the sharpest band in the hyperspectral image cube. The reference band is normalized to match the variations found in the base image. The implementation here follows the descriptions given in previous studies.[3]

More specifically, the sharper reference image, I_{ref}, is normalized with respect to the image to be sharpened or base image, I_{base}, by subtracting its mean and scaling by the ratio of the standard deviation of I_{base} to the standard deviation of I_{ref}, then adding the mean of I_{base}:

$$I_{ref} = \frac{I_{ref} - \mu(I_{ref})}{\sigma(I_{base})/\sigma(I_{ref})} + \mu(I_{base})$$

A low pass filtered image of I_{ref} is obtained through butterworth filtering as I_{low}, the high-pass filter image I_{high} is then obtained as

$$I_{high} = I_{ref} \oslash (I_{low} + \epsilon)$$

and lastly the the sharpened image, I_{sharp}, is obtained by the following haddmard product as

$$I_{sharp} = I_{base} \circ I_{high}$$

2.5 Multi-resolution Analysis by Wavelets

Wavelets are mathematical functions often used to analyze and process signals and images. They are potent tools in signal processing, data compression, and image analysis.[16]

Wavelet decomposition is a method used in image processing to remove noise and extract features. The process involves breaking down an image into low and high-frequency components at different levels of detail using filters. The low-frequency component is further decomposed into four sub-bands at each level: approximation, horizontal detail, vertical detail, and diagonal detail. The process continues until the desired level of detail is reached. The wavelet coefficients obtained from the decomposition process can be used for various tasks such as compression, feature extraction, and denoising.[17]

Let us assume we have an image I with dimensions $M \times N$. The 2D wavelet decomposition involves applying filters to the image in horizontal and vertical directions. The low-pass filter (LPF) extracts the low-frequency components, while the high-pass filter (HPF) extracts the high-frequency components. With image

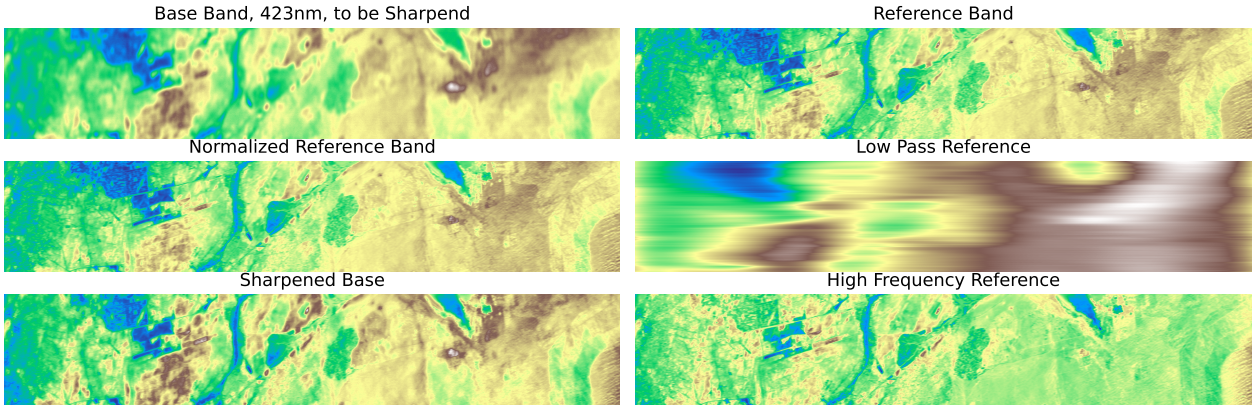

Figure 4: The various steps of enhancing the sharpness of an image by the use of a Laplacian pyramid approach

I, resulting in the low-frequency coefficients L and high-frequency coefficients H in the horizontal, vertical and diagonal direction,

$$L = \mathrm{LPF}(I)$$
$$H = \mathrm{HPF}(I).$$

The resulting coefficients should then be arranged into a 2D matrix, representing the wavelet decomposition of the image, commonly expressed as

$$W_m = \begin{bmatrix} L & H_h \\ H_v & H_d \end{bmatrix}$$

The dimensions of W_m are identical to the original image I. The process is repeated on the low-frequency image L to get to the next level. Certain conditions need to be satisfied for it to be a valid wavelet transformation. The mother wavelets must exhibit admissibility, regularity, orthogonality, and similarity.

The admissibility condition ensures that the wavelet is compact in frequency and has zero mean. Mathematically, this condition is expressed as:

$$\int_{-\infty}^{\infty} |\hat{\psi}(\omega)|^2 \frac{d\omega}{\omega} < \infty$$

where $\hat{\psi}(\omega)$ is the Fourier transform of the wavelet function $\psi(t)$. This condition guarantees that the continuous wavelet transform (CWT) is invertible and allows for accurate reconstruction of the original signal or image. The regularity condition states that the wavelet function should have smoothness and concentration in both time and frequency. This condition ensures that the wavelet function has a well-defined shape and can effectively capture the details of the signal or image. Furthermore, in some applications, wavelets are required to be orthogonal. Orthogonal wavelets have the property that the inner product between any two wavelets is zero. Lastly, The similarity condition requires that the wavelet function exhibit similarity or self-similarity at different scales. This property allows for the efficient representation of signals or images with varying levels of detail.

A wavelet can be a family of functions obtained by scaling and translating a single function called the mother wavelet. The mother wavelet is a function localized in both time and frequency domains, meaning it has a finite duration and bandwidth. Scaling and translating the mother wavelet produces functions with different scales and positions across the signal or image, creating the family of wavelets. Applying Wavelet analysis can improve the sharpness of an image given a reference image. This technique involves using wavelets to extract high-frequency information from a blurry band image and then enhancing the Image'simage's sharpness.

The basic idea is to decompose the blurry band image into the various wavelet coefficients at different levels and then use these coefficients to estimate the high-frequency information missing in the blurry band image. The wavelet coefficients of the sharpest band image or neighboring sharpest band can be used to estimate the high-frequency information in the missing detail images in the blurry band image that has been decomposed as an approximation image. This is the decomposition of the sharp reference band and the baseband, the band to be sharpened, which can then be used to enhance the overall sharpness of the image cube. In fig. 5, a three-level wavelet decomposition of the Parana River is included for illustrative purposes.

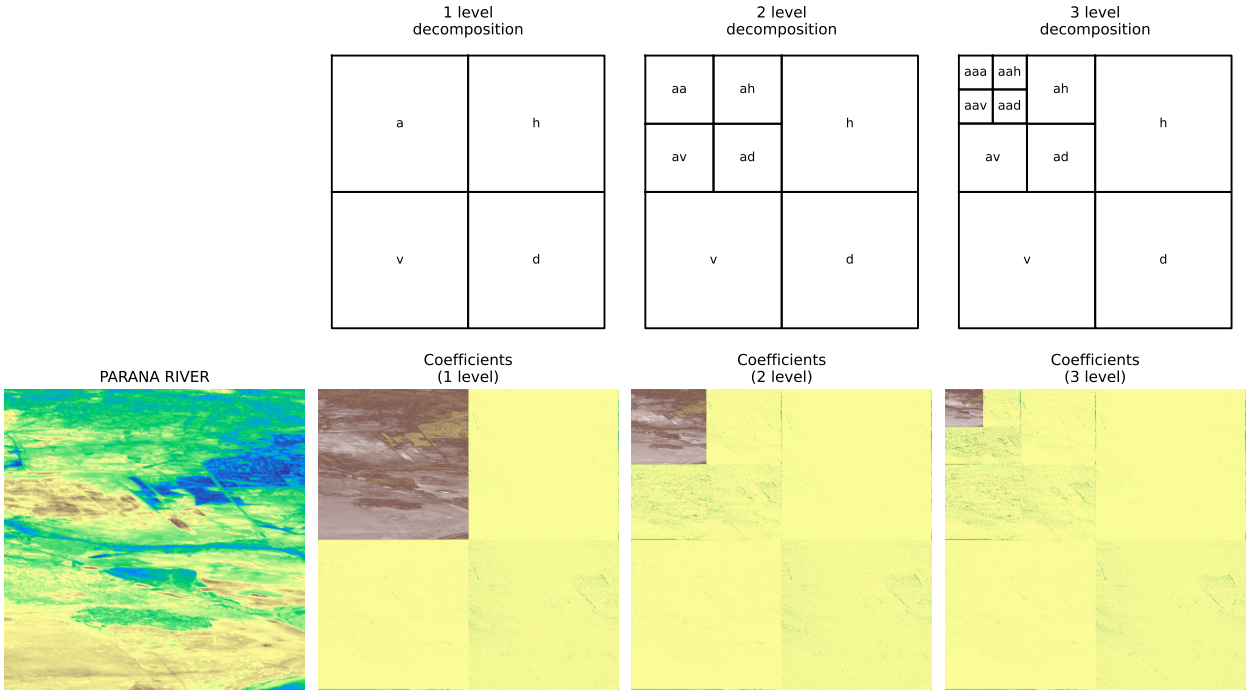

Figure 5: Three-level wavelet decomposition of Parana River. Alongside the normalized full-size image, the depth of the wavelet decomposition increases level by level towards the right. Each level makes a new set of approximation and detail images from the previous level.

3. METHODOLOGY

This section provides an overview of the experimental setup used to test and validate the proposed methods. Data from HYPerspectral Small satellite for ocean Observation (HYPSO)-1 is used in the qualitative assessment of the algorithms given in section 4.

The parameters used for the different Wavelet transformations are namely different mother wavelets, being *Daubechies*, *Haar*, *Symlet*, and *Coiflets*[17] ran at one to three different decomposition levels. The best performing from each family at the best performing level is given in section 4.

The quantitative evaluation uses data from other sensors. The data are simulated from historical hyperspectral images. The images are collected from two different missions, EO-1 and PRISMA, in total, three scenes. The image capture process is simulated by modeling a camera directly above each scene, and ray tracing from the pixels onto the camera sensor, according to the sensor's pixel footprint function (PFF). Two images are created for each scene, one in which the PFF is constant for all wavelengths and a second in which its size increases at the edges of the spectrum. This is done to simulate the optical aberrations in miniaturized push-broom imagers with a *center wavelength* being sharper than the rest.

Three different methods to evaluate the performance of the algorithms are given below: No-reference based methods that look at the intrinsic properties of an image The aggregated results for an image cube A method that relies on a reference value to compare with

3.1 Spatial quality evaluation by BRISQUE

Image Quality Assessment (IQA) is an essential task in image processing. It's used to evaluate the quality of an image after it's been distorted in some way, such as through compression, noise, or blur. Here IQA is used to see if the image has been enhanced without an available reference. In this article, the NR (No-Reference) IQA model called the Blind/Referenceless Image Spatial Quality Evaluator, or BRISQUE is used to evaluate the blurriness of an image. BRISQUE is an IQA model that is not dependent on the distortion apparent in the image for natural scenes and operates in the spatial domain. The model is based on natural scene statistics. It is derived empirically based on statistics from other images, whereas this work uses the model from OpenCV.[18]

Unlike other NR IQA models, BRISQUE uses the scene statistics of locally normalized luminance coefficients to measure the loss of "naturalness", that is, to which extent pixels follow a normal distribution after a localized normalization procedure in the image caused by distortions. The original BRISQUE paper[18] demonstrates that the metric can have certain advantages over the full-reference peak signal-to-noise ratio and the structural similarity index.

An illustration of the BRISQUE score for different images is given in fig. 6. The BRISQUE score is computed for the entire scene, but the images show a sub-image of the Kuwait scene given in fig. 1.

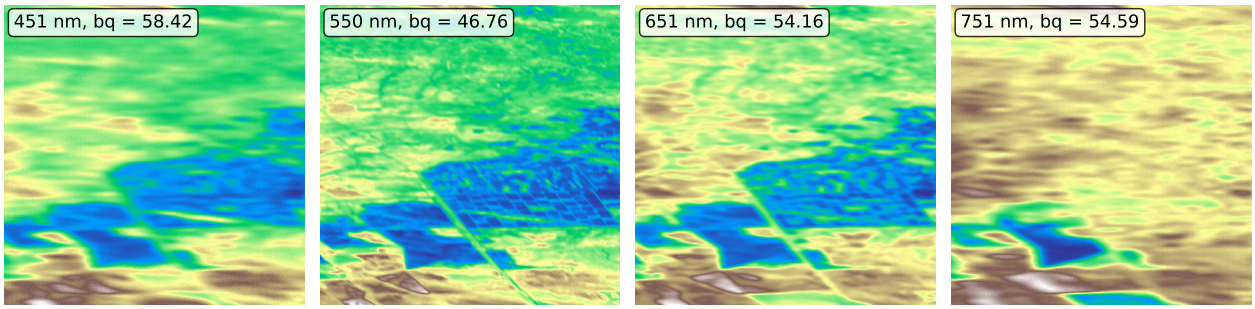

Figure 6: The BRISQUE Score for the Kuwait scene at different wavelengths. The score is abbriviated *bq*. A lower score indicates a more *natural looking* image. The score is computed for the entire scene, and a sub-image is displayed to portray the details of the scene better.

The score of this metric ranges from 0 to 100, with a lower value being desirable, and is demonstrated to indicate which band in the hyperspectral image cube can be perceived as the sharpest. Although BRISQUE was not specifically developed for nor calibrated on remote sensing images, it enables the detection of generic image distortions that affect any digital imaging pipeline, such as thermal noise, blur, and optical aberrations.

3.2 Perceived Line Spread Function (PLSF)

The PLSF, in addition to the global metric, is also used manually to identify edges in various HYPSO-1 images to assess the sharpness of a band. This evaluation is a continuation of previous work that assessed which camera parameters provided the optimal spatial resolution that the HYPSO-1 imager could provide.[2] The Line Spread Function (LSF) is a concept of the blurriness of an image resulting from the imaging system. This function is defined as the imaging system's response to an infinitely long and infinitely thin line. Thus, the LSF is a one-dimensional function that shows how light intensity is distributed along a line perpendicular to the direction of the line object. How many pixels a sure edge takes up can then be used as a proxy for the spatial resolvability of an image, i.e., the sharpness. Here, this function is estimated based on manually selected edges occurring in natural images and used to determine the spatial resolution of the hyperspectral image cubes before and after an intervention. This function is also used to indicate which bands are the sharpest.

3.3 Spectral Angle Mapper

The Spectral Angle Mapper (SAM) is a frequently used metric in hyperspectral image analysis.[1] If a spatial pixels is viewed as a vector with all the different wavelengths as its elements, then the SAM score is the angle between these two vectors. We can use the dot product formula to compute the angle between two vectors. Let $\vec{a}$ and $\vec{b}$ be the two vectors in $\mathbb{R}^n$. Then, the angle θ between them is given by

$$\theta = \cos^{-1}\left(\frac{\vec{a}\cdot\vec{b}}{\|\vec{a}\|\|\vec{b}\|}\right),$$

where $\vec{a}\cdot\vec{b}$ is the dot product of $\vec{a}$ and $\vec{b}$, and $\|\vec{a}\|$ and $\|\vec{b}\|$ are the magnitudes of $\vec{a}$ and $\vec{b}$, respectively. The main advantage of SAM over other basic distortion measures, such as RMSE, is that it is less sensitive to shadows and wavelength-independent variations in luminance in the scene.

4. RESULTS AND DISCUSSION

This section provides the plots resulting from testing the different sharpening methods. We note that more wavelet-based sharpening methods were tested than what is presented here. Due to their performance, a subset of four combinations of mother wavelets and decomposition levels is given here. The name of the mother wavelet is given before the dash, and the level of decomposition is given after the dash. Beyond that, the PCA-CS refers to Principal Component Analysis based Component Substitution. Lastly, the name Laplacian refers to the approach using the Laplacian pyramid, and the baseline is the original image. For all sharpening-algorithms, the sharpest band has been selected to be 555 nanometers for the HYPSO-1 images.

Violin plots have been used to show the summary statistics of the applied methods. A violin plot is a type of data visualization that combines a box plot with a kernel density plot to show the distribution of numerical data. It helps compare summary statistics, such as the median and interquartile range, while showing the entire data distribution, including any peaks or modes.

The results from the simulated scenes are given in figs. 7a and 7b as a set of violin plots. In the case of the SAM metric found in fig. 7b, the image cube that is used as the truth is simply the image cube before the blurring effect is added. The results from the HYPSO-1 scenes are given in figs. 8a and 8b as another set of violin plots. While the sharpening is somewhat quantified in this section, it is essential to remember that we are only quantifying the perceived sharpness of the images.

The mean average of the estimated FWHM and BRISQUE score for the HYPSO-1 Images for different sharpening algorithms as a function of wavelength can be seen in fig. 9 and fig. 10, respectively.

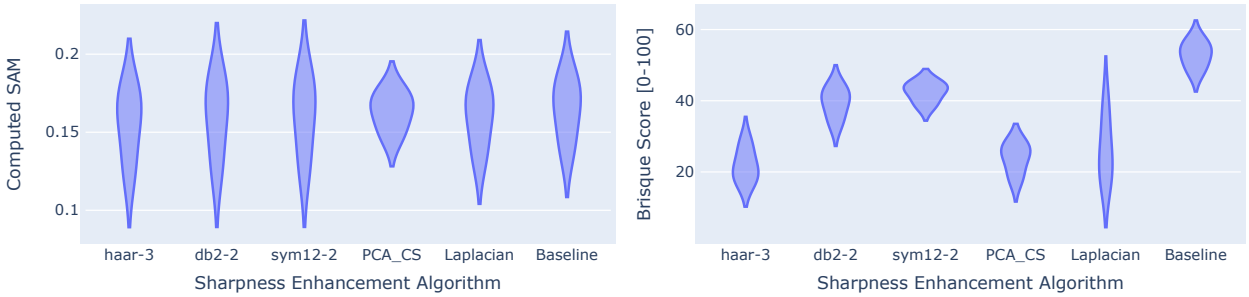

(a) SAM Metric on the simulated scenes (b) BRISQUE Metric on the simulated scenes

Figure 7: Violin Plot for the simulated scenes.

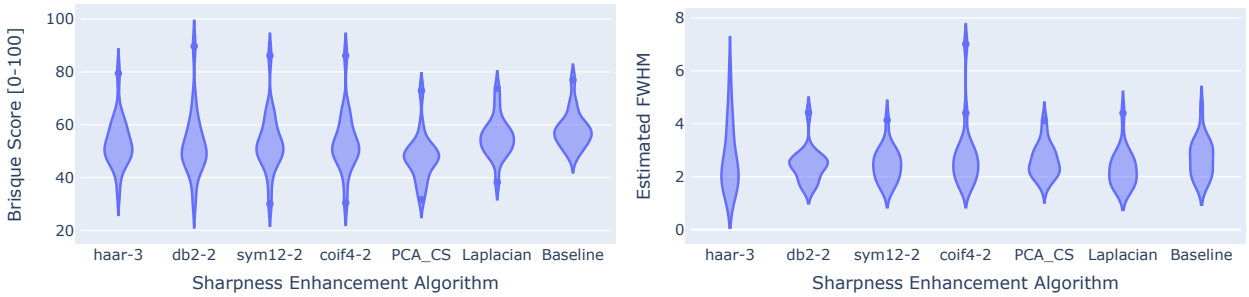

(a) BRISQUE Metric on the HYPSO-1 scenes. (b) Estimated FWHM on the HYPSO-1 scenes.

Figure 8: Violin Plot for the HYPSO-1 scenes.

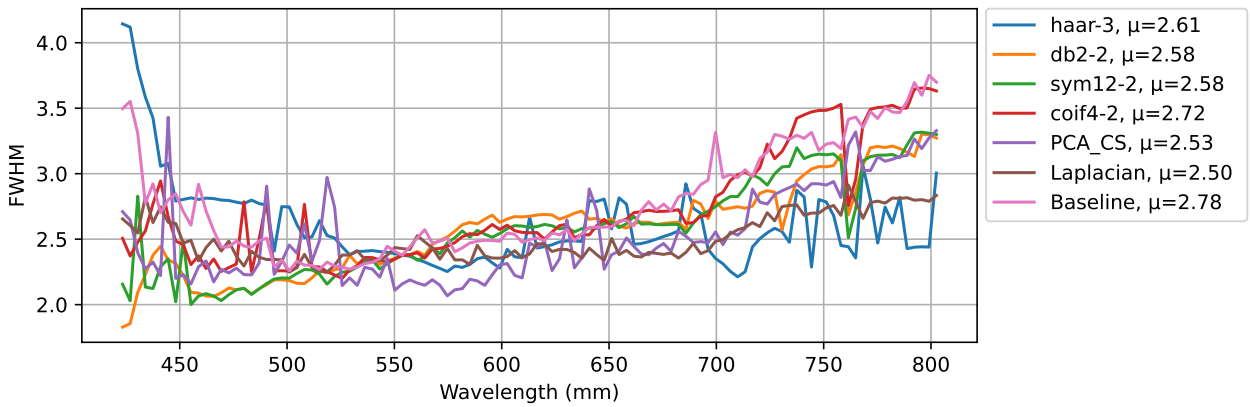

Figure 9: The mean average of the estimated FWHM for the HYPSO-1 Images for different sharpening algorithms as a function of wavelength.

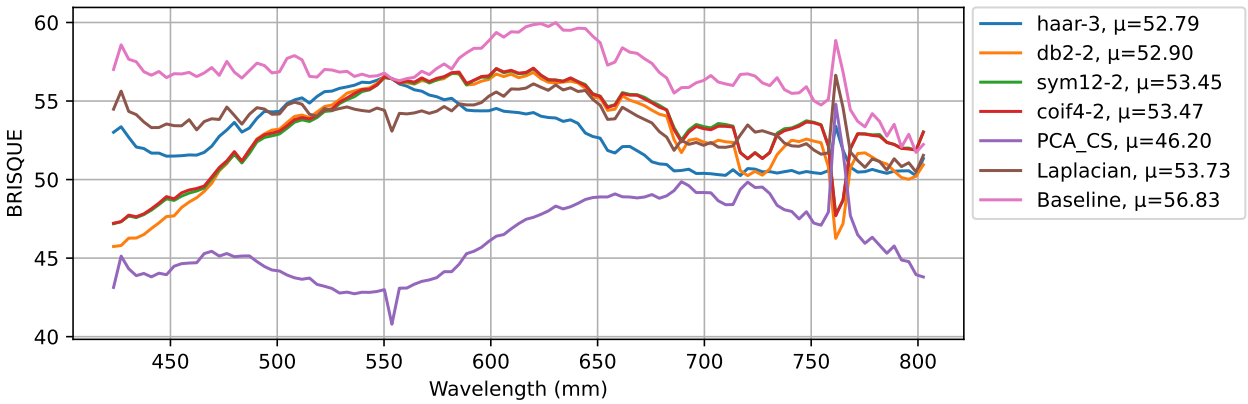

Figure 10: The mean average of the BRISQUE score for the HYPSO-1 Images for different sharpening algorithms as a function of wavelength.

Lastly, a visualization of how the different sharpening algorithms perform is given in fig. 11. This figure shows how the different algorithms alter the original data and indicate how the different artifacts present at the given wavelengths can sometimes be transmitted from the reference image to other parts of the electromagnetic spectrum.

4.1 Limitations and Interpretations

In terms of the BRISQUE Score, the baseline mean average given in fig. 8a and fig. 7a appear to have a smaller range than the image cubes exhibit for the various algorithms used. From fig. 8a, it appears that the different wavelet-based sharpening algorithms produce image cubes that exhibit a spatial image quality per the BRISQUE score across an extensive range but that the majority of the images lie close to the performance of the other sharpening algorithm families. In fig. 11, some artifacts from the sharper reference image seem to be carried over into other bands as well, and perhaps especially so for the wavelet transform. This carrying over of sharpening artifacts could cause the BRISQUE score to provide more favorable results without the spectral image features one is looking for being improved.

From fig. 10, it is clear that all of the sharpening algorithms improve the apparent spatial quality of the image in terms of the BRISQUE metric. Interestingly, for the Wavelet-based methods, the sharpening is limited to the reference band. In contrast, the reference band also appears to be sharpened for the Laplacian and component substitution. The performance of the component substitution in terms of the BRISQUE metric is significantly better for most wavelengths on average, as can be seen in fig. 10. However, from fig. 11, the component substitution appears to impose more of the artifacts from the selected center band into the sharpened bands than, for example, the Laplacian approach in the same anecdotal illustration. As a result of this duality, the choice of sharpening, algorithm will naturally depend on the intended end-use, whether the spectral fidelity is of utmost importance or if the spatial resolvability needs to take priority.

None of the sharpening algorithms perform considerably differently regarding the estimated FHWM in fig. 9. From the figure, the component substitution gives the best improvement in estimated FWHM for the wavelengths closest to the reference wavelength. On average, the Laplacian approach gives an improvement in terms of the estimated FWHM across all wavelengths. In this regard, some of the wavelengths are greatly improved by using component substitution. However, at the same time, other parts of the spectrum are significantly degraded, leading to a poor mean average performance for this approach. The various Wavelets perform similarly to the other methods, and the *db2-2* and *sym12-2* appear to give an improved estimated FWHM for the wavelengths lower than the reference image and poorer performance for the wavelengths higher than the reference image. This variation in performance for the wavelets could be related to how the different wavelengths correlate for a given scene; that is, if the edge being enhanced is prominent in both the blurry band and the reference band, the wavelets would provide a good improvement, but in the other case it will have the opposite effect.

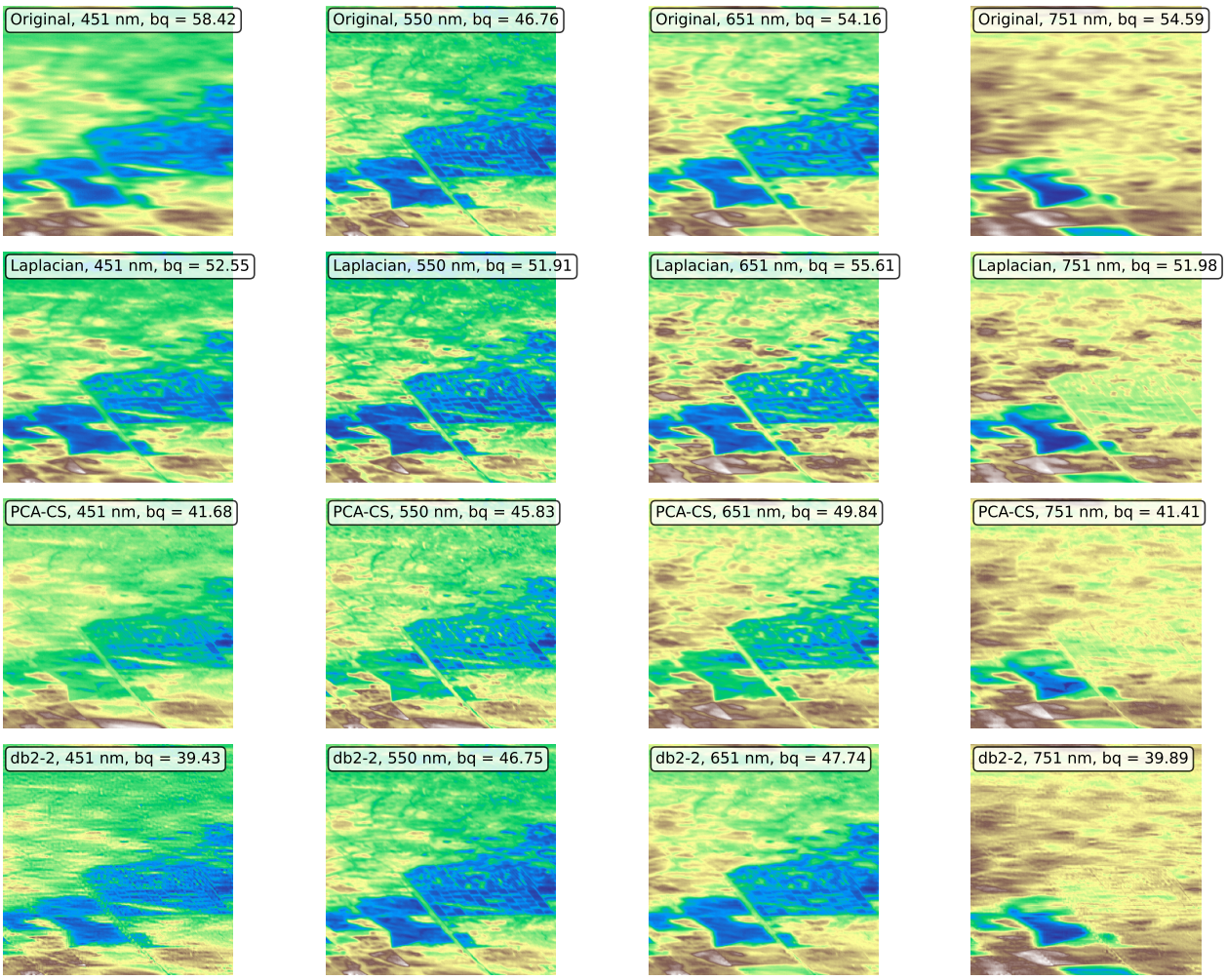

Figure 11: A visualization of one representative from all families of sharpening algorithms used here with the original image at different wavelengths. Alongside the image, the BRISQUE score for the full cube that they produce is given as well, denoted as *bq*. A sub-image is displayed to portray spatial details of the scene better.

In the aforementioned figures, there is some evidence that a single reference band does not best sharpen the wavelength-dependent blur observed in image cubes from miniaturized push-broom hyperspectral imagers. That is, the spatial resolvability of the reference band relative to the blurry band will affect the overall performance, as indicated in the past.[11] Thus, it would be an exciting topic for future research to investigate strategies to incorporate more of the apriori knowledge of the nature of the observed optical aberrations.

This work mainly concerns adapting classical methods for spatial sharpening of Earth Observation data. A consequence of this is that new and novel approaches, relying more heavily on modern machine learning such as,[19,20] are not included in the evaluation presented here. It is reasonable to expect that these methods could be adapted to the type of optical aberrations that are focused on here and beyond. This study uses a limited data set, and a more extensive data set could have strengthened the conclusions. This extends to both the simulated and the real-world data set. The number of wavelets transformation shown in this study is limited. Albeit the transformations tested here yielded near identical results, it is fair to assume that a more extensive analysis and potential further adaptations and modifications to the suggested approach could have resulted in better performance.

5. CONCLUSIONS AND FUTURE WORK

This body of work evaluates different spatial sharpening algorithms for Earth Observation data from a single camera using the BRISQUE score and estimated FWHM under the assumption of wavelength-dependent blur found in miniaturized hyperspectral push-broom sensors. The results show that all sharpening algorithms improve the spatial quality of the image in terms of the BRISQUE metric, but the choice of algorithm depends on the intended end-use. The Laplacian approach gives the best improvement in terms of estimated FWHM across all wavelengths. In contrast, in this regard, the component substitution approach performs significantly better for most wavelengths on average. However, the component substitution approach imposes more artifacts from the selected center band into the sharpened bands than the Laplacian approach. The various wavelets perform similarly to the other methods regarding estimated FWHM. An exciting way forward is to incorporate more apriori knowledge of the nature of observed optical aberrations to improve the overall performance of spatial sharpening algorithms. The study mainly concerns adaptations of classical methods for spatial sharpening, and new and novel approaches relying more heavily on modern machine learning are not included in the evaluation. Lastly, a more extensive dataset and analysis could have strengthened the conclusions, but the presented results provide the basis for further development.

Acknowledgment

This work was supported by the Research Council of Norway through the Centre of Excellence funding scheme NTNU AMOS (grant no. 223254), HYPSCI (grant no. 325961), and Green-Platform (grant no. 328724), NO Grants 2014 - 2021 under Project ELO-Hyp (contract no. 24/2020). The authors would also like to thank the full HYPSO-1 team, including all students that have been a part of the project, NanoAvionics for support with the satellite, and KSAT for extra downlink opportunities through the KSATlite network.

REFERENCES

[1] Eismann, M., "Hyperspectral remote sensing," in [*Hyperspectral Remote Sensing*], Society of Photo-Optical Instrumentation Engineers (2012).

[2] Langer, D. D., Johansen, T. A., and Sørensen, A. J., "Consistent along track sharpness in a push-broom imaging system," in [*IGARSS 2023 - IEEE International Geoscience and Remote Sensing Symposium*], (July 2023).

[3] Loncan, L., De Almeida, L. B., Bioucas-Dias, J. M., Briottet, X., Chanussot, J., Dobigeon, N., Fabre, S., Liao, W., Licciardi, G. A., Simoes, M., et al., "Hyperspectral pansharpening: A review," *IEEE Geoscience and remote sensing magazine* **3**(3), 27–46 (2015).

[4] Sigernes, F., Mikko Syrjäsuo, Storvold, R., Fortuna, J., Grøtte, M. E., and Johansen, T. A., "Do it yourself hyperspectral imager for handheld to airborne operations," *Opt. Express* **26**, 6021–6035 (Mar 2018).

[5] Prentice, E. F., Grøtte, M. E., Sigernes, F., and Johansen, T. A., "Design of a hyperspectral imager using COTS optics for small satellite applications," in [*Proc. SPIE 11852, International Conference on Space Optics – ICSO 2020, 1185258*], (2021).

[6] Mao, Y., Betters, C. H., Evans, B., Artlett, C. P., Leon-Saval, S. G., Garske, S., Cairns, I. H., Cocks, T., Winter, R., and Dell, T., "Openhsi: A complete open-source hyperspectral imaging solution for everyone," *Remote Sensing* **14**(9) (2022).

[7] Loizzo, R., Guarini, R., Longo, F., Scopa, T., Formaro, R., Facchinetti, C., and Varacalli, G., "Prisma: The italian hyperspectral mission," in [*IGARSS 2018 - 2018 IEEE International Geoscience and Remote Sensing Symposium*], 175–178 (2018).

[8] Aasen, H., Honkavaara, E., Lucieer, A., and Zarco-Tejada, P. J., "Quantitative remote sensing at ultra-high resolution with uav spectroscopy: A review of sensor technology, measurement procedures, and data correction workflows," *Remote Sensing* **10**(7) (2018).

[9] Aiazzi, B., Baronti, S., and Selva, M., "Improving component substitution pansharpening through multivariate regression of ms +pan data," *IEEE Transactions on Geoscience and Remote Sensing* **45**(10), 3230–3239 (2007).

[10] Davis, C. O., Kavanaugh, M., Letelier, R., Bissett, W. P., and Kohler, D., "Spatial and spectral resolution considerations for imaging coastal waters," in [*Coastal Ocean Remote Sensing*], **6680**, 196 – 207, SPIE (2007).

[11] Yokoya, N., Grohnfeldt, C., and Chanussot, J., "Hyperspectral and multispectral data fusion: A comparative review of the recent literature," *IEEE Geoscience and Remote Sensing Magazine* **5**(2), 29–56 (2017).

[12] Fortuna, J., Martens, H., and Johansen, T. A., "Multivariate image fusion: A pipeline for hyperspectral data enhancement," *Chemometrics and Intelligent Laboratory Systems* **205**, 104097 (2020).

[13] Vivone, G., Garzelli, A., Xu, Y., Liao, W., and Chanussot, J., "Panchromatic and hyperspectral image fusion: Outcome of the 2022 whispers hyperspectral pansharpening challenge," *IEEE Journal of Selected Topics in Applied Earth Observations and Remote Sensing* **16**, 166–179 (2023).

[14] Bakken, S., Henriksen, M. B., Birkeland, R., Langer, D. D., Oudijk, A. E., Berg, S., Pursley, Y., Garrett, J. L., Gran-Jansen, F., Honoré-Livermore, E., Grøtte, M. E., Kristiansen, B. A., Orlandic, M., Gader, P., Sørensen, A. J., Sigernes, F., Johnsen, G., and Johansen, T. A., "Hypso-1 cubesat: First images and in-orbit characterization," *Remote Sensing* **15**(3) (2023).

[15] Bourke, P., "Histogram Matching — paulbourke.net." http://paulbourke.net/miscellaneous/equalisation/ (2011). [Accessed 15-08-2023].

[16] Palsson, F., Sveinsson, J. R., Ulfarsson, M. O., and Benediktsson, J. A., "Model-based fusion of multi- and hyperspectral images using pca and wavelets," *IEEE Transactions on Geoscience and Remote Sensing* **53**(5), 2652–2663 (2015).

[17] Gonzalez, R. C., [*Digital image processing*], Pearson education india (2009).

[18] Mittal, A., Moorthy, A. K., and Bovik, A. C., "No-reference image quality assessment in the spatial domain," *IEEE Transactions on Image Processing* **21**(12), 4695–4708 (2012).

[19] Huang, S. and Messinger, D. W., "An unsupervised laplacian pyramid network for radiometrically accurate data fusion of hyperspectral and multispectral imagery," *IEEE Transactions on Geoscience and Remote Sensing* **60**, 1–17 (2022).

[20] Huang, S. and Messinger, D., "An unsupervised cascade fusion network for radiometrically-accurate vis-nir-swir hyperspectral sharpening," *Remote Sensing* **14**(17) (2022).